ISSN 1573-160X, *PHYSICAL OCEANOGRAPHY*, Vol. 33, Iss. 1, pp. 33-47 (2026)
Original Russian Text © A. E. Korinenko, V. V. Malinovsky, 2026,
published in *Morskoy Gidrofizicheskiy Zhurnal*, 2025, Vol. 42, Iss. 1, pp. 37–52

Original article

Retrieval of Surface Current Velocities and their Shears Using the Shipborne *X*- and *Ka*-Band Radar Data

A. E. Korinenko ✉, V. V. Malinovsky

Marine Hydrophysical Institute of RAS, Sevastopol, Russian Federation
✉ *korinenko.alex@yandex.ru*

Abstract
Purpose. The purpose of the study is to develop a method for retrieving the surface current velocity vector and determining its vertical shear from the sea surface radar images obtained at low grazing angles under a wide range of meteorological conditions.
Methods and Results. The presented results were obtained during the comprehensive field experiments conducted at the Black Sea Hydrophysical Subsatellite Polygon of Marine Hydrophysical Institute. The experiments included the use of coherent marine radar systems MRS-1011 (*X* band) and MRS-3000 (*Ka* band), which were deployed at a stationary oceanographic platform and operated in a circular scanning mode with horizontal transmit/receive polarization. Sea surface observations were carried out at grazing incidence angles. Radar imaging was simultaneously accompanied by a set of field measurements at the platform, which included recording the current velocity magnitude and direction at different depths and sea surface elevation, as well as meteorological parameter measurements. The surface current velocity vector was retrieved using cross-spectral analysis of the time series of radar images. This approach enables one to construct a dispersion curve whose deformation is used to estimate the surface current velocity. Aliasing correction in the second Nyquist zone expanded the spectral range of the analyzed wave field, which is particularly important in regions with weak currents and for assessing the vertical shear of current velocities.
Conclusions. The feasibility of applying marine navigation radars to determine the current velocity vector in the coastal zone within a radius of several kilometers has been confirmed. The surface current velocity amplitudes calculated using radar data generally agree with the values obtained from current measurements by an acoustic Doppler current profiler. The vertical current shear in the upper ocean layer was assessed. It is shown that under weak and moderate winds, the dimensionless current shear remains constant, and with increasing wind speed, it decreases. The obtained results are in satisfactory agreement both with the field measurement data and previously published studies.

Keywords: remote sensing, radar images, sea surface, dispersion relation, surface current velocity, vertical shear of current velocity, field measurements, aliasing

Acknowledgements: The study was supported by a Russian Science Foundation grant No. 24-27-20105 (https://rscf.ru/project/24-27-20105), and by an Agreement with the Department of Education and Science of Sevastopol No. 85 dated June 19, 2024. The authors are grateful to V.N. Kudryavtsev, who proposed the method for determining the vertical shear of the current velocity using radar data and developed the algorithm for its implementation.

For citation: Korinenko, A.E. and Malinovsky, V.V., 2026. Retrieval of Surface Current Velocities and their Shears Using the Shipborne *X*- and *Ka*-Band Radar Data. *Physical Oceanography*, 33(1), pp. 33-47.

Introduction

The study of surface currents plays a vital role in addressing a wide range of scientific, economic, and environmental challenges. Measurements of the current velocity magnitude and direction are typically conducted using Acoustic Doppler

Current Profilers (ADCP) or Lagrangian drifters. Coastal waters, characterized by high spatiotemporal variability of surface currents, require a comprehensive approach to monitoring water dynamics [1]. In this regard, standard measurements are often supplemented by remote sensing techniques. Among the most widely used tools in such research are high-frequency radar systems [2, 3] and microwave radar stations [4, 5].

Modern marine radar systems are all-weather instruments offering high spatial and temporal resolution. Depending on the objectives, they can be deployed on offshore platforms, vessels, or coastal structures. When operating in a circular scan mode, these radar systems can provide continuous radar coverage of the sea surface within a radius of up to 10 km.

The formation of radar images of the sea surface is significantly influenced by the modulation of scattering elements by long surface gravity waves and shadowing effects, which together enable the visualization of the surface wave structure.

To retrieve surface current velocities from nautical radar data, a three-dimensional Fourier transform of a sequence of radar images is applied. This approach allows for the construction of a dispersion curve, and the surface current velocity is estimated based on its deformation [6]. This method has been successfully employed in oceanographic research for over four decades [4, 7–9] and has been implemented in the commercial system WaMoS II [10].

In [8, 11, 12] the effectiveness of using shipborne nautical radars for monitoring coastal currents at distances of up to 7 km from the shoreline was confirmed. Further advancements in radar technology, particularly the development of solid-state coherent microwave radars, have opened new prospects for estimating surface current velocities by analyzing the Doppler velocities of scatterers [13].

In addition to conventional algorithms based on three-dimensional Fourier transforms, cross-spectral analysis has recently gained traction for determining surface current velocities. This technique has been successfully used to estimate currents from optical satellite data [14, 15]. The effectiveness of the cross-spectral method for retrieving surface current velocities from nautical radar data was demonstrated in [16].

It should be noted that shipborne radars, such as those operating in the X-band, can provide information on mean current velocities in the upper ocean layer with a thickness of several meters [8, 11, 12, 16].

To study processes affecting the intensity of turbulent mixing in the near-surface layer, information on the vertical structure of currents may be of particular importance. One of the few studies in this area is [17], which presents vertical current velocity profiles in the 2–8 m layer reconstructed from shipborne radar data.

The purpose of the study is to develop a method for retrieving surface current velocity vectors [16] from radar data by extending the spectral range of the studied wave field into the second Nyquist zone, and to apply this approach to studying and estimating vertical current shear in the upper layer of the sea.

Experimental conditions and data processing methodology

The field experiment was conducted from August to December of 2022–2024 at the stationary oceanographic platform of the Black Sea Hydrophysical Sub-Satellite Polygon of Marine Hydrophysical Institute (MHI), Russian Academy of Sciences.

Radar measurements were carried out using two short-range coherent radar systems with high range resolution – MRS-1011 and MRS-3000 (manufactured by JSC *Micran* Research and Production Company, Tomsk). The technical specifications of the radar systems are presented in the table.

Technical parameters of radar systems

Parameter	Radar Systems	
	MRS-1011 (*X*-band)	MRS-3000 (*Ka*-band)
Transmit power	not more than 1 W	not more than 250 mW
Wave length	3.2 cm	0.8 cm
Transmitted signal	Continuous wave with linear-frequency modulation (LFM)	
Antenna beamwidth in vertical/horizontal planes	30°/1°	
Transmit/receive polarization	Horizontal/horizontal	
Operating mode	Circular scanning	
Antenna rotation period (T_{RL})	2.24 s	2.53 s

The radars were installed on the oceanographic platform at heights of 14 m (MRS-1011) and 12.4 m (MRS-3000) above sea level (Fig. 1). During the experiment, the systems operated in a circular scan mode. Due to the specific placement of the radars on the platform, the sea surface observation sector for MRS-1011 was 55–315° (geographic azimuth), and for MRS-3000 – 0–220° and 330–360°. In 2022, measurements were performed simultaneously using both radar systems, whereas in 2023–2024, only the MRS-3000 radar was employed. The duration of radar measurements was at least 5 minutes, corresponding to a sequence of 120 or more radar images.

To convert the relative units of the radar signal into absolute values of the normalized radar cross-section (NRCS, σ_0), the results given in [18] were used.

Wind speed V and direction φ_V were recorded using a Davis Vantage Pro2 6152 weather station installed at a height of 23 m above sea level. Surface wave characteristics were measured using a string wave gauge. Processing of the wave gauge data yielded frequency spectra of sea surface elevations and enabled the determination of spectral peak frequencies f_p and corresponding spectral peak wavelengths $\lambda_p = g/(2\pi f_p^2)$.

In 2024, current velocity was measured using an acoustic Doppler current profiler of the WHM1200 series (operating frequency 1200 kHz, manufactured by RDI, USA). The instrument was bottom-mounted at a depth of 24 m, 50 m away from the platform, and oriented vertically upward. The measurements provided current velocity profiles over a 22 m-thick layer with a vertical resolution of 1 m. The averaging interval was 1 min. Data from near-surface horizons (depths less than 2 m) were excluded from the analysis due to significant errors caused by the presence of air bubbles in the surface layer (generated by breaking wind waves) and acoustic signal reflections from the water–air interface.

F i g. 1. Stationary oceanographic platform of the Black Sea Hydrophysical Subsatellite Polygon of Marine Hydrophysical Institute, RAS:*1, 3* – MRS-1011 and MRS-3000 radar systems, respectively; *2* – meteorological measurement system; *4* – string wave gauge

Surface current velocity retrieval methodology. In the present study, the cross-spectral analysis method applied to sequences of radar images [16] is employed to retrieve surface current velocities. For this purpose, each radar image sequence was transformed from polar coordinates onto a regular grid with a spatial step of $\Delta x = \Delta y = 1$ m. Fig. 2 shows fragments of radar images obtained on November 6, 2022, using two radar systems. The shoreline of Golubaya Bay is clearly visible in the images. During the measurements, an easterly wind with a speed of 16 m/s was observed. The solid blue areas in the images correspond to shadowing by platform structures, in these sectors, the radar transmitter was switched off. The red squares in Fig. 2 highlight the image segments (each 470 × 470 m²) used for surface current velocity retrieval. The well-defined wave structure observed in the radar panoramas results from the modulation of scatterers by long surface gravity waves [19, 20]. This enables the application of spectral methods to analyze fragments of radar panoramas in order to determine the spectral composition and propagation direction of the waves, as well as to estimate surface current velocities.

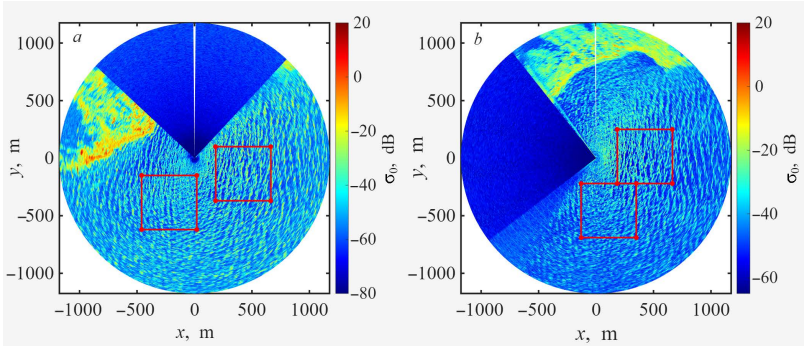

F i g. 2. Radar images of the sea surface obtained by MRS-1011 (*a*) and MRS-3000 (*b*). The brightness scale corresponds to the normalized radar cross section (NRCS) of the sea surface

We define the cross-spectrum $S_{i,i+1}(\mathbf{k})$ between each pair of consecutive radar images I_i and I_{i+1} $(i = 1,2, \dots, n-1)$ and calculate the average over the entire set of $n-1$ cross-spectra:

$$S_{ac}(\mathbf{k}) = \frac{1}{n-1}\sum_{i=1}^{n-1} S_{i,i+1}(\mathbf{k}). \quad (1)$$

A significant cross-spectral characteristic is the coherence function, defined as:

$$\gamma^2(\mathbf{k}) = \frac{|S_{ac}(\mathbf{k})|^2}{S_{aa}^{(1,n-1)}(\mathbf{k})S_{aa}^{(2,n)}(\mathbf{k})},$$

where $S_{aa}(\mathbf{k}) = \frac{1}{n}\sum_{i=1}^{n} S_{i,i}(\mathbf{k})$, $S_{i,i}(\mathbf{k})$ is the autospectrum for each radar image I_i.

Cross-spectral analysis allows one to determine the phase shift between the spectral harmonics of two successive radar images and, given the antenna rotation period, to estimate the frequencies ω of these harmonics:

$$\omega(k_x, k_y) = -\Phi\big(k_x, k_y\big)/T_{\mathrm{RL}}, \quad (2)$$

where T_{RL} is the antenna rotation period; $\Phi(k_x, k_y) = \arg(S_{ac}(\mathbf{k}))$ is the phase spectrum.

The frequencies obtained from formula (2) that correspond to surface gravity waves lie in the region defined by the dispersion relation:

$$\omega_0 = \sqrt{gk\cdot\tanh(kH)}, \quad (3)$$

where g is the acceleration due to gravity; k is the wavenumber magnitude; H is the water depth. Note that the water depth at the study sites exceeded 40 m. Typical spectral peak wavelengths under storm conditions ranged from 50 to 80 m. In this case, $\tanh(kH) \cong 1$; therefore, the finite-depth correction to the dispersion relation in formula (3) was neglected.

In the presence of surface currents, the frequencies are shifted due to the Doppler effect, and dispersion relation (3) becomes:

$$\omega = \omega_0 + k\tilde{U}(k)\cos\Delta\varphi, \quad (4)$$

where $\widetilde{U}(k)$ is the magnitude of the effective surface current velocity [21]; $\Delta\varphi = \varphi_w - \varphi_{\widetilde{U}}$ is the angle between the wave vector and the current; φ_w is the wave propagation direction; $\varphi_{\widetilde{U}}$ is the surface current direction. Depending on the current direction, the measured ω lie either above or below the theoretical ω_0.

In the present work, to estimate $\widetilde{U}(k)$ and $\varphi_{\widetilde{U}}$, the phase spectrum $\Phi(k_x, k_y)$ was divided into 16 angular sectors with a step of 22.5°. In sectors where $\Phi(k_x, k_y)$ satisfied the criterion $\gamma^2(k_x, k_y) > 0.4$ [16, 19], dispersion curves were constructed and fitted with expression (4). This yields a set of radial surface current velocity components $U_j^r(\varphi_w^j, \varphi_{\widetilde{U}}) = \widetilde{U}(k)\cos\Delta\varphi_j$, where j is the sector index; φ_w^j is the mean wave direction in the j-th sector. If the number of sectors for which $U_j^r(\varphi_j, \varphi_{\widetilde{U}})$ was calculated exceeded 3, these data were used for the subsequent retrieval of $\widetilde{U}$ and $\varphi_{\widetilde{U}}$.

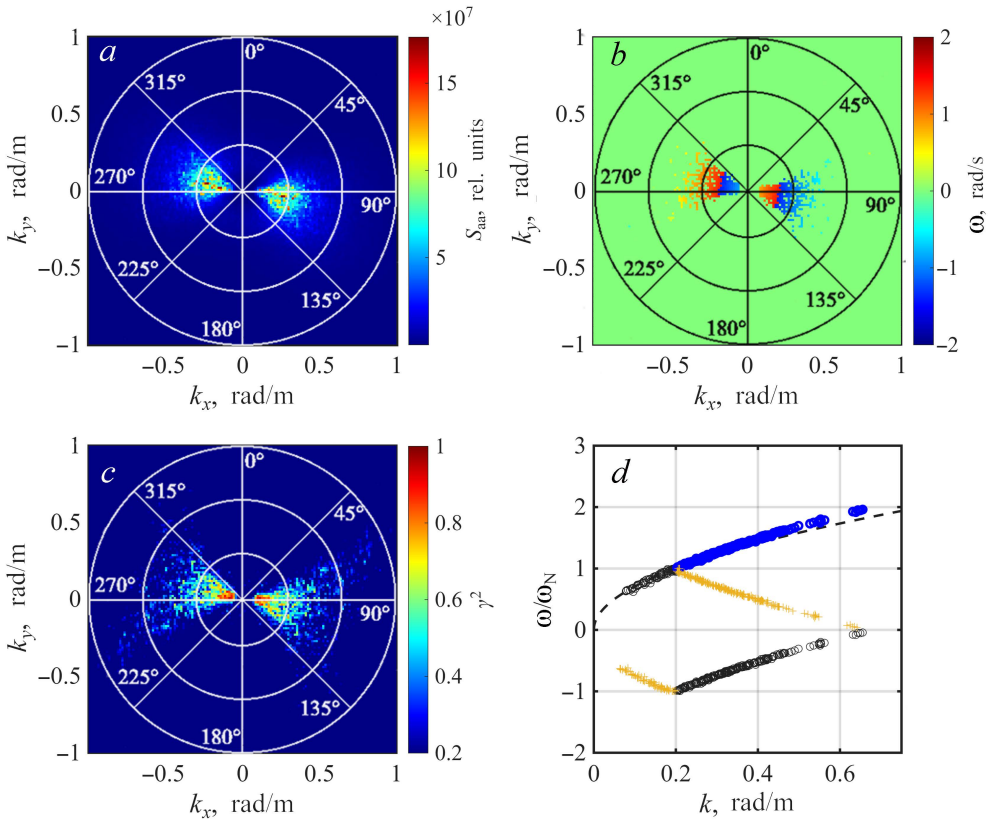

F i g. 3. Spectral analysis of radar images: *a* – radar autospectrum; *b* – phase spectrum; *c* – coherence function; *d* – dispersion curve normalized by ω_N. The data were obtained on November 6, 2022 at 15:00 under a wind speed of 16 m/s and a wind direction of 100°

Validation of the surface current vector retrieval method. As an example, Fig. 3 presents the results of applying spectral analysis to a sequence of 130 radar images obtained using the MRS-1011 system. Fig. 3, a shows the radar autospectrum $S_{aa}(k_x, k_y)$, with the color scale on the right representing spectral

values in arbitrary units. Fig. 3, *b* displays the phase spectrum, where, for clarity, the color scale corresponds to the frequencies ω determined according to formula (2). It should be noted that Fig. 3, *b* shows only the ω values for which $\gamma^2 > 0.4$. As can be seen from the presented results, sequential radar images exhibit a high degree of correlation, confirmed by the large γ^2 values (Fig. 3, *c*). As expected, the autospectrum $S_{aa}(k_x, k_y)$ demonstrates mirror symmetry, while the phase spectrum is antisymmetric. The phase spectrum enables the determination of the spectral composition of the waves, and the sign of the frequency ω uniquely establishes the wave propagation direction.

The relatively low rotation speed of the radar antennas imposes limitations on the spectral range of the wave field that can be retrieved. In our experiments, the antenna of the MRS-1011 radar completed a full revolution in 2.24 s, corresponding to a Nyquist angular frequency of $\omega_N = \pi/T_{\mathrm{RL}} = 1.40$ rad/s; the MRS-3000 antenna had a rotation period of 2.53 s, corresponding to $\omega_N = 1.24$ rad/s.

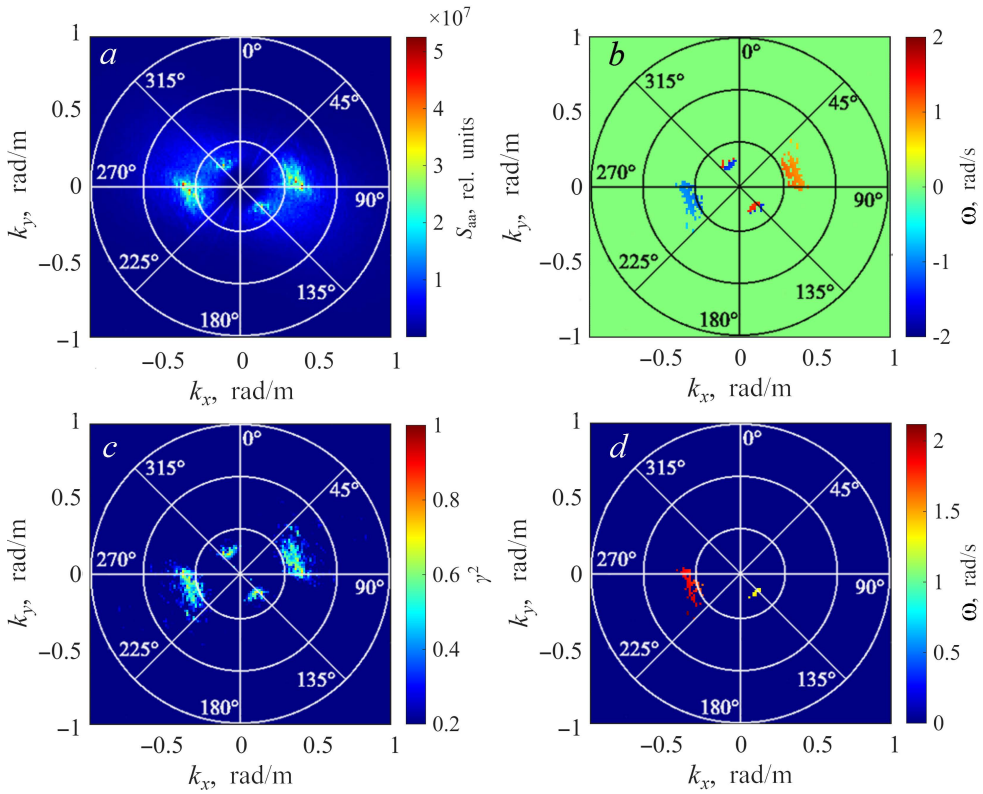

F i g. 4. Spectral analysis of radar images: *a* – radar autospectrum; *b*, *d* – phase spectrum; *c* – coherence function. The data were obtained on October 26, 2022, at 16:00, under a wind speed of 10 m/s and a wind direction of 250°

Frequencies of surface waves with $\omega > \omega_N$, determined by formula (2), are subject to frequency aliasing, which is clearly illustrated in Fig. 3, *b*. The magnitude

of ω increases up to ω_N, and upon exceeding this value, becomes negative. For the symmetric part of $\omega(k_x, k_y)$, the opposite pattern is observed: ω takes negative values, and upon reaching $-\omega_N$, the frequency ω becomes positive.

These patterns are most clearly represented in Fig. 3, *d*, which shows the dependence of ω/ω_N on the wavenumber. The black circles correspond to the dispersion curve affected by aliasing; the orange crosses represent the symmetric part of $\omega(k)$; the dashed line shows the dependence ω_0/ω_N.

In [22, 23] an approach for reconstructing true frequencies in the range $\omega \in (\omega_N, 2\omega_N)$ was proposed. According to this method, the true frequency value is determined as $\omega + \omega_{RL}$, where $\omega_{RL} = 2\pi/T_{RL}$. The reconstructed frequencies are shown in Fig. 3, *d* as blue circles. It is evident that the black circles (for $\omega \in (0, \omega_N)$) and the blue circles cluster around the dispersion curve.

Applying this procedure makes it possible to extend the spectral range of the analyzed wave field to waves with lengths down to ~ 9 m, which is particularly important for regions with weak current velocities. It should be noted that this approach has been successfully applied in [24, 25].

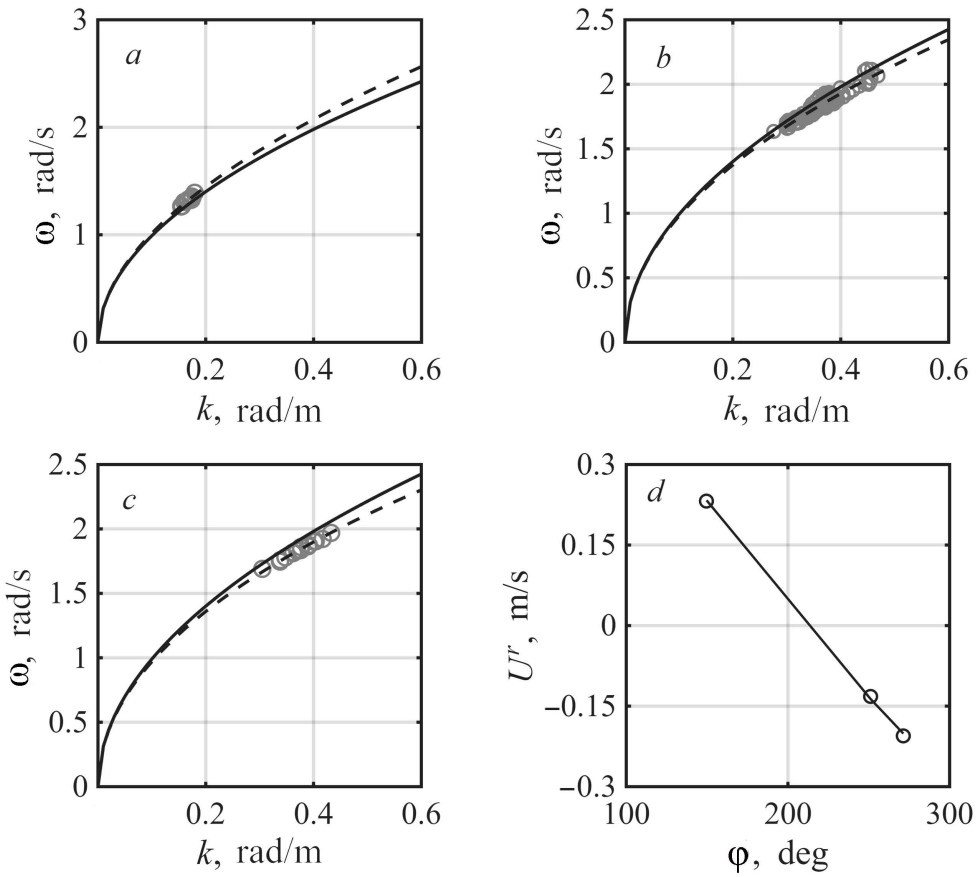

F i g. 5. Dispersion relations for the data shown in Fig. 4 within the angular sectors 135–157.5° (*a*), 247.5–270° (*b*), 270–292.5° (*c*); *d* – dependence of radial velocity on the wave propagation direction

Field measurements are typically conducted under mixed sea conditions, where wind waves and swell are present simultaneously. It is important to note that the propagation directions of swell and wind waves may differ significantly. The surface current vector retrieval methodology requires dedicated validation under such conditions. Fig. 4 presents the processing results of MRS-1011 radar data acquired in the presence of swell. As in Fig. 3, sequential images exhibit high correlation, confirmed by the large coherence γ^2 values (Fig. 4, *c*). Fig. 4, *d* shows the phase spectrum corrected for aliasing in the range $\omega \in (\omega_N, 2\omega_N)$. Analysis of the figure allows one to identify two wave systems: wind waves from the western direction and swell waves from the southeastern direction.

We estimate $\widetilde{U}(k)$ and $\varphi_{\widetilde{U}}$ using the data presented in Fig. 4. In the analysis, three angular sectors were identified (the angular ranges are indicated in the caption of Fig. 5); for each sector, a dispersion curve was constructed and the radial component of the surface current velocity U^r was determined. Figs. 5, *a–c* show the results of this analysis. The solid line shows the dependence (3), and the dashed line shows the dependence (4), where the values $U^r = \widetilde{U}(k)\cos\Delta\varphi$ were determined using the least squares method. The values of U^r for the mean wave directions in the considered angular sectors are presented in Fig. 5, *d*. Negative values of U^r indicate that the current direction is opposite to the wave propagation direction.

The solid line in Fig. 5, *d* corresponds to the dependence $U^r = \widetilde{U}\cos(\varphi_w - \varphi_{\widetilde{U}})$, where the values $\widetilde{U} = 0.25$ m/s and $\varphi_{\widetilde{U}} = 5.38$ rad (308°) were determined by the least squares method. In this case, the retrieved current is directed against the propagation of wind waves but coincides with the propagation direction of the swell.

Discussion of results

In 2022, surface current velocity was simultaneously retrieved using *X*-band and *Ka*-band radar data. Analysis of the data revealed no differences between the $\widetilde{\mathbf{U}}$ values obtained from the two radar systems. In the subsequent analysis, we do not distinguish between the types of radar used for surface current velocity retrieval.

A total of 174 series of radar measurements were analyzed for wind speeds ranging from 8 to 24 m/s. The mean standard deviation of the retrieved $\widetilde{U}$ was 0.03 m/s. Only measurements with surface current velocities exceeding 0.06 m/s were used for further analysis.

To compare the obtained results with ADCP measurements correctly, it is necessary to estimate the depth to which the current velocity retrieved from radar data corresponds. For deep water, the effective velocity $\widetilde{\mathbf{U}}(k)$ represents a weighted average [21]:

$$\widetilde{\mathbf{U}}(k) = 2k\int_0^\infty \mathbf{U}(z)\exp(-2kz)\,dz, \qquad (5)$$

where $\mathbf{U}(z)$ is the vertical profile of the current velocity vector, with the positive *z*-axis directed downward.

According to expression (5), for **U**(z) the dominant influence of the weighting coefficient $\exp(-2kz)$ is determined mainly by values in the upper layer of the sea. For further data analysis, we employ the empirical estimate [21], according to which

the radar averages the current velocity over a layer of thickness $h_k \approx 1/(2k)$. Thus, longer waves are influenced by currents at greater depths compared to shorter waves.

As follows from Fig. 5, the radial velocity was estimated from dispersion curves within a given wavenumber range. For each value of U^r, the mean wavenumber $\bar{k}$ and the corresponding depth $h_{\bar{k}}$ were calculated. According to our estimates, $h_{\bar{k}}$ varied in the range 1–2.8 m, and the mean value over all measurement series was $\langle h_{\bar{k}} \rangle = 1.6$ m. To compare $\widetilde{U}$ with the current profiler results, ADCP data from the closest reliable horizon, 2.2 m, were used.

Fig. 6 compares the current speed retrieved from radar data with that measured by the ADCP at the 2.2 m horizon. The retrieved current speed $\widetilde{U}$ varied within the range of 0.06–0.62 m/s. The straight line in Fig. 6 shows the linear dependence $\widetilde{U} = a + bU$, where the coefficients were determined by the least squares method: $a = 0.07$ m/s is the offset of the line relative to the line of equal values, the slope is $b = 0.95$, and the root-mean-square deviation between the indicated pairs of values is 0.08 m/s.

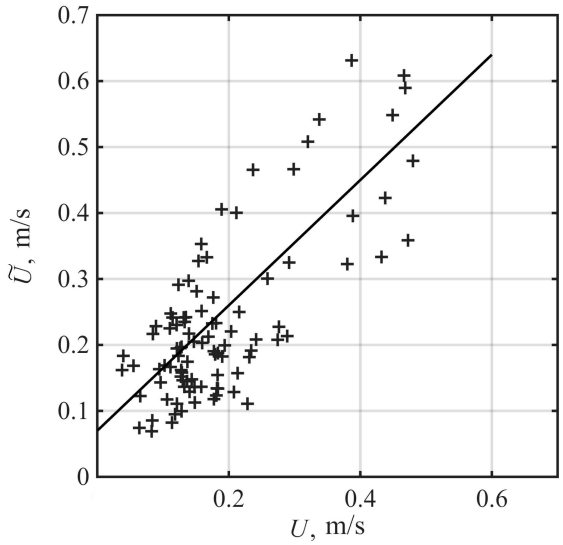

F i g. 6. Current velocity magnitude (crosses) derived from radar data and ADCP measurements. The straight line corresponds to the relationship $\widetilde{U}$ = 0.07 + 0.95U

The difference observed in Fig. 6 between $\widetilde{U}$ and the current velocity measured by the ADCP may be associated with the difference in the definition of these quantities. The current velocity measured by the current profiler is an average value over a 1 m-thick layer centered at a depth of 2.2 m. At the same time, the radar-derived values $\widetilde{U}$ represent weighted averages over the layer from $z = 0$ m to $z \approx 1.6$ m. As is known, the greatest velocity shear is observed precisely in the near-surface layer. Thus, the values of $\widetilde{U}$ may systematically exceed the ADCP data, as follows from Fig. 6.

Estimation of vertical velocity shear. As shown above, the modified radar image processing technique used in this paper allows obtaining $\omega(k)$ over a wide wavenumber range (Figs. 3, *d*; 5). We demonstrate that, in addition to determining

mean current velocities, it becomes possible to estimate vertical shears of drift currents from the dispersion curves.

Indeed, taking into account expression (5), it can be shown that the mean gradient of $\widetilde{U}$ over the measured wavenumber range is equal to the mean gradient of the current velocity $\langle z\frac{\partial U}{\partial z}\rangle$ over the layer of thickness $1/(2\bar{k})$:

$$-\langle k\frac{\partial \widetilde{U}}{\partial k}\rangle = \langle z\frac{\partial U(z)}{\partial z}\rangle = \langle 2k\int_0^\infty z\frac{\partial U(z)}{\partial z}\exp(-2kz)\,dz\rangle. \quad (6)$$

The quantity $\langle k\frac{\partial \widetilde{U}}{\partial k}\rangle$ can be obtained using expression (2), from which it follows:

$$\frac{\partial \omega}{\partial k} = \frac{\partial \omega_0}{\partial k} + \widetilde{\mathbf{U}}(\mathbf{k}) + k\frac{\partial \widetilde{\mathbf{U}}(\mathbf{k})}{\partial k}. \quad (7)$$

We assume that $\widetilde{\mathbf{U}}$ is a superposition of the coastal current (not related to the local wind forcing), the wind-driven current $\mathbf{u}_w$, and the Stokes drift $\mathbf{u}_{\mathrm{St}}$. The coastal current velocity is considered constant with depth. For waves propagating downwind, the change in the mean wind-drift velocity over the measured k range, according to formula (7), can be written as:

$$\langle k\frac{\partial u_w}{\partial k}\rangle = \langle\frac{\partial \omega}{\partial k}\rangle - c_{g0}(\bar{k}) - \langle U^r\rangle - \langle k\frac{\partial u_{\mathrm{St}}}{\partial k}\rangle, \quad (8)$$

where $\langle\frac{\partial \omega}{\partial k}\rangle$ is the mean value of the variation of ω over the k range measured by the radar; $c_{g0}(\bar{k})$ is the theoretical group velocity for the mean wavenumber $\bar{k}$; $\langle U^r\rangle$ is the projection of the mean current velocity onto the wind direction obtained from the dispersion curve; $\langle k\frac{\partial u_{\mathrm{St}}}{\partial k}\rangle$ is the mean gradient of the Stokes drift. Using wave gauge measurements, $\langle k\frac{\partial u_{St}}{\partial k}\rangle$ was calculated for wind waves in the 1.6 m layer.

Thus, by applying the methodology [16] to a sequence of radar images and using expression (8), it is possible to estimate the mean drift current shear over a layer of thickness $h_{\bar{k}}$, which under our conditions varied between 1 and 2.8 m.

Of particular interest is the behavior of the vertical current gradient under different wind conditions. Considering formula (6), we examine the dependence of the dimensionless quantities $\langle\frac{\partial u_w}{\partial \ln k}\rangle/V$, shown by crosses in Fig. 7, on wind speed. The wind speed range (6–28 m/s) is divided into 9 intervals with a step $\Delta V = 2.5$ m/s. The mean values of $\langle\frac{\partial u_w}{\partial \ln k}\rangle/V$ calculated within each interval $(V, V+\Delta V)$ are shown in Fig. 7 by circles; vertical lines indicate the standard deviations.

The straight line in Fig. 7 marks the value $\langle\frac{\partial U}{\partial \ln z}\rangle/V = 0.004$, specific to a near-wall turbulent boundary layer, in which the velocity profile is logarithmic: $\frac{\partial U}{\partial \ln z} = v_*/\kappa$. Here $\kappa = 0.4$ is the von Kármán constant; $v_* = \sqrt{\rho_a/\rho_w}\,u_*$ is the friction velocity in water; ρ_a is the air density; ρ_w is the water density; $u_* = C_D^{1/2}V$ is the friction velocity in air; and $C_D = 0.002$ is the drag coefficient.

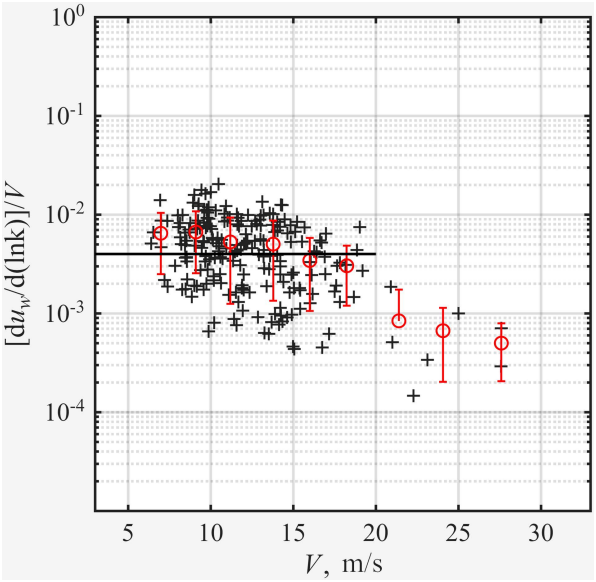

F i g. 7. Wind dependence of the dimensionless vertical current speed gradient

As follows from Fig. 7, at $V \lesssim$ 12–13 m/s, the obtained values of $\langle\frac{\partial u_w}{\partial \ln k}\rangle /V$ are, within the confidence intervals, close to the parameter 0.004. Despite the scatter of the experimental data, a clear tendency toward a decrease in the vertical current velocity gradient with increasing wind speed is evident. The values of $\langle\frac{\partial u_w}{\partial \ln k}\rangle /V$ decrease from 0.006 to 0.0005 as the wind speed increases over the range of 13–28 m/s.

According to experimental data [26] obtained using Lagrangian drifters in the vicinity of the stationary oceanographic platform, current velocity gradients just below the surface are 2–5 times weaker than those in a logarithmic boundary layer. To explain these observations, a semi-empirical model was proposed in [26], in which the reduction in vertical velocity shear compared to the logarithmic boundary layer is attributed to increased turbulence intensity in the upper layer of the sea due to wind-wave breaking.

Conclusions

This paper presents the results of retrieving surface current velocities from *X*-band and *Ka*-band radar surveys conducted at low grazing angles of observation of the sea surface. The studies were carried out in 2022–2024 in the waters of the Black Sea Hydrophysical Sub-Satellite Polygon of Marine Hydrophysical Institute, Russian Academy of Sciences. The data processing methodology is based on the analysis of cross-spectra of a sequence of sea surface radar images.

The relatively low rotation rate of the radar antennas imposes limitations on the determination of dispersion relations. Particular attention is paid to accounting for the aliasing effect that occurs when calculating the frequencies of wind waves whose frequencies exceed the antenna rotation period of the radar. It is shown that the values of the wind wave frequency retrieved from radar data and the circular

frequency of antenna rotation make it possible to eliminate the aliasing effect and extend the dispersion relation up to a wavenumber of 0.7 rad/m.

Based on radar data, dispersion relations for wind waves were obtained and compared with the theoretical dependence for the case of no current. The values of $\widetilde{U}$ were determined from the magnitude of their difference. The magnitudes of the retrieved surface current velocities ranged from 0.06 to 0.6 m/s with a standard deviation of ± 0.03 m/s.

The radar-derived $\widetilde{U}$ values are somewhat higher than the current velocities at a depth of 2.2 m obtained from ADCP measurements. This difference may be attributed to the fact that $\widetilde{U}$ represents a weighted average of the current velocity over the 0–1.6 m layer, where the greatest velocity shear is observed.

Estimates of vertical current shear in the upper layer of the sea were performed. It was found that at wind speeds below 12–13 m/s, the dimensionless current velocity gradient is close to a constant value of 0.006, and with increasing wind speed it decreases to 0.005 at 28 m/s.

REFERENCES

1. Zatsepin, A.G., Gorbatskiy, V.V., Myslenkov, S.A., Shpilev, N.N., Dudko, D.I., Ivonin, D.V., Silvestrova, K.P., Baranov, V.I., Telegin, V.A. [et al.], 2017. Comparison of Coastal Currents Measured by HF and X-Band Radars with ADCP and Drifter Data at the IO RAS Hydrophysical Test Site in the Black Sea. *Sovremennye Problemy Distantsionnogo Zondirovaniya Zemli iz Kosmosa*, 14(7), pp. 250-266. https://doi.org/10.21046/2070-7401-2017-14-7-250-266 (in Russian).
2. Huang, W., Wu, S., Gill, E., Wen, B. and Hou, J., 2002. HF Radar Wave and Wind Measurement over the Eastern China Sea. *IEEE Transactions on Geoscience and Remote Sensing*, 40(9), pp. 1950-1955. https://doi.org/10.1109/TGRS.2002.803718
3. Wyatt, L.R., Green, J.J., Middleditch, A., Moorhead, M.D., Howarth, J. and Holt, M., 2006. Operational Wave, Current, and Wind Measurements with the Pisces HF Radar. *IEEE Journal of Oceanic Engineering*, 31(4), pp. 819-834. https://doi.org/10.1109/JOE.2006.888378
4. Nieto Borge, J.C. and Guedes, C., 2000. Analysis of Directional Wave Fields Using X-Band Navigation Radar. *Coastal Engineering*, 40(4), pp. 375-391. https://doi.org/10.1016/S0378-3839(00)00019-3
5. Horstmann, J., Borge, J.C.N., Seemann, J., Carrasco, R. and Lund, B., 2015. Wind, Wave, and Current Retrieval Utilizing X-Band Marine Radars. In: Y. Liu, H. Kerkering and R. H. Weisberg, eds., 2015. *Coastal Ocean Observing Systems*. London: Academic Press, pp. 281-304. https://doi.org/10.1016/B978-0-12-802022-7.00016-X
6. Young, I.R., Rosenthal, W. and Ziemer, F., 1985. A Three-Dimensional Analysis of Marine Radar Images for the Determination of Ocean Wave Directionality and Surface Currents. *Journal of Geophysical Research: Oceans*, 90(C1), pp. 1049-1059. https://doi.org/10.1029/JC090iC01p01049
7. Senet, C.M., Seemann, J., Flampouris, S. and Ziemer, F., 2007. Determination of Bathymetric and Current Maps by the Method DiSC Based on the Analysis of Nautical X-Band Radar Image Sequences of the Sea Surface (November 2007). *IEEE Transactions on Geoscience and Remote Sensing*, 46(8), pp. 2267-2279. https://doi.org/10.1109/TGRS.2008.916474
8. Ivonin, D.V., Telegin, V.A., Bakhanov, V.V., Ermoshkin, A.V. and Azarov, A.I., 2011. Sample Application of a Low-Cost X-Band Monitoring System of Surface Currents at the Black Sea Shore. *Russian Journal of Earth Sciences*, 12(2), ES2003. https://doi.org/10.2205/2011ES000507
9. Lund, B., Graber, H.C., Tamura, H., Collins, C.O. and Varlamov, S.M., 2015. A New Technique for the Retrieval of Near-Surface Vertical Current Shear from Marine X-Band Radar Images. *Journal of Geophysical Research: Oceans*, 120(12), pp. 8466-8486. https://doi.org/10.1002/2015JC010961

10. Hessner, K.G., Nieto-Borge, J.C. and Bell, P.S., 2008. Nautical Radar Measurements in Europe: Applications of WaMoS II as a Sensor for Sea State, Current and Bathymetry. In: V. Barale and M. Gade, eds., 2008. *Remote Sensing of the European Seas*. Dordrecht, the Netherlands: Springer, pp. 435-446. https://doi.org/10.1007/978-1-4020-6772-3_33

11. Ivonin, D.V., Chernyshov, P.V., Kuklev, S.B. and Myslenkov, S.A., 2016. Preliminary Comparisons of Sea Current Velocity Vector Measurements by a Nautical X-Band Radar and Moored ADCP. *Sovremennye Problemy Distantsionnogo Zondirovaniya Zemli iz Kosmosa*, 13(2), pp. 53-66. https://doi.org/10.21046/2070-7401-2016-13-2-53-66 (in Russian).

12. Ivonin, D.V., Telegin, V.A., Azarov, A.I., Ermoshkin, A.V. and Bakhanov, V.V., 2011. Possibility to Measure Velocity Vector of Surface Currents by Means of Nautical Radar with Wide Beamwidth Antenna. *Sovremennye Problemy Distantsionnogo Zondirovaniya Zemli iz Kosmosa*, 8(4), pp. 219-227 (in Russian).

13. Ermoshkin, A.V., Kapustin, I.A., Molkov, A.A. and Bogatov, N.A., 2020. Determination of the Sea Surface Current by a Doppler X-band Radar. *Fundamentalnaya i Prikladnaya Gidrofizika*, 13(3), pp. 93-103. https://doi.org/10.7868/S2073667320030089 (in Russian).

14. Kudryavtsev, V.N., Yurovskaya, M., Chapron, B., Collard, F. and Donlon, C., 2017. Sun Glitter Imagery of Surface Waves. Part 1: Directional Spectrum Retrieval and Validation. *Journal of Geophysical Research: Ocean*, 122(2), pp. 1369-1383. https://doi.org/10.1002/2016JC012426

15. Kudryavtsev, V.N., Yurovskaya, M., Chapron, B., Collard, F. and Donlon, C., 2017. Sun Glitter Imagery of Surface Waves. Part 2: Waves Transformation on Ocean Currents. *Journal of Geophysical Research: Ocean*s, 122(2), pp. 1384-1399. https://doi.org/10.1002/2016JC012426

16. Chen, Z., Zhang, B., Kudryavtsev, V., He, Y. and Chu, X., 2019. Estimation of Sea Surface Current from X-Band Marine Radar Images by Cross-Spectrum Analysis. *Remote Sensing*, 11(9), 1031. https://doi.org/10.3390/rs11091031

17. Lund, B., Graber, H.C., Tamura, H., Collins, C.O. and Varlamov, S.M., 2015. A New Technique for the Retrieval of Near-Surface Vertical Current Shear from Marine X-band Radar Image. *Journal of Geophysical Research: Oceans*, 120(12), pp. 8466-8486. https://doi.org/10.1002/2015JC010961

18. Korinenko, A.E. and Malinovsky, V.V., 2025. Wind Field Retrieval in the Coastal Zone Using X-Band Radar Data at Large Incidence Angles. *Ecological Safety of Coastal and Shelf Zones of Sea*, (1), pp. 26-41 (in Russian).

19. Plant, W.J., 1989. The Modulation Transfer Function: Concept and Applications. In: Komen, G.J. and Oost, W.A., eds., 1989. *Radar Scattering from Modulated Wind Waves.* Dordrecht, the Netherlands: Springer, pp. 155-172. https://doi.org/10.1007/978-94-009-2309-6_13

20. Kudryavtsev, V.N., Hauser, D., Caudal, G. and Chapron, B., 2003. A Semiempirical Model of the Normalized Radar Cross Section of the Sea Surface, 2. Radar Modulation Transfer Function. *Journal of Geophysical Research: Oceans*, 108(C3), 8055. https://doi.org/10.1029/2001JC001004

21. Stewart, R.H. and Joy, J.W., 1974. HF Radio Measurements of Surface Currents. *Deep Sea Research*, 21(12), pp. 1039-1049. https://doi.org/10.1016/0011-7471(74)90066-7

22. Seemann, J. and Ziemer, F., 1995. Computer Simulation of Imaging Ocean Wave Fields with a Marine Radar. In: IEEE, 1995. *Oceans '95. MTS/IEEE Conference Proceedings "Challenges of Our Changing Global Environment"*. San Diego, CA, USA. Vol. 2, pp. 1128-1133. https://doi.org/10.1109/OCEANS.1995.528583

23. Seemann, J., Ziemer, F. and Senet, C.M., 1997. A Method for Computing Calibrated Ocean Wave Spectra from Measurements with a Nautical X-Band Radar. In: IEEE, 1997. *Oceans '97. MTS/IEEE Conference Proceedings "500 Years of Ocean Exploration"*. Halifax, NS, Canada. Vol. 2, pp. 1148-1154. https://doi.org/10.1109/OCEANS.1997.624154

24. Senet, C.M., Seemann, J. and Ziemer, F., 1997. An Iterative Technique to Determine the near Surface Current Velocity from Time Series of Sea Surface Images. In: IEEE, 1997. *Oceans '97. MTS/IEEE Conference Proceedings "500 Years of Ocean Exploration"*. Halifax, NS, Canada. Vol. 1, pp. 66-72. https://doi.org/10.1109/OCEANS.1997.634337

25. Lund, B., Collins, C.O., Graber, H.C., Terrill, E. and Herbers, T.H., 2014. Marine Radar Ocean Wave Retrieval's Dependency on Range and Azimuth. *Ocean Dynamics*, 64(7), pp. 999-1018. https://doi.org/10.1007/s10236-014-0725-6

26. Kudryavtsev, V., Shrira, V., Dulov, V. and Malinovsky, V., 2008. On the Vertical Structure of Wind-Driven Sea Currents. *Journal of Physical Oceanography*, 38(10), pp. 2121-2144. https://doi.org/10.1175/2008JPO3883.1

Submitted 04.07.2025; approved after review 05.08.2025;
accepted for publication 10.11.2025.

About the authors:

Aleksandr E. Korinenko, Senior Researcher, Marine Hydrophysical Institute of RAS (2 Kapitanskaya Str., Sevastopol, 299011, Russian Federation), CSc. (Phys.-Maths.), **ORCID ID: 0000-0001-7452-8703**, **Scopus Author ID: 23492523000**, **SPIN-code: 7288-8023**, korinenko.alex@yandex.ru

Vladimir V. Malinovsky, Senior Researcher, Marine Hydrophysical Institute of RAS (2 Kapitanskaya Str., Sevastopol, 299011, Russian Federation), CSc. (Phys.-Maths.), **ORCID ID: 0000-0002-5799-454X**, **Scopus Author ID: 23012976200**, **ResearcherID: F-8709-2014**, **SPIN-code: 9206-3020**, vladimir.malinovsky@mhi-ras.ru

Contribution of the co-authors:

Aleksandr E. Korinenko – development of techniques and carrying out the experimental studies, analysis and synthesis of the research results, preparation of the text of the article

Vladimir V. Malinovsky – development of experimental research method, analysis and synthesis of research results, participation in the discussion of the article materials, preparation of the article text

The authors have read and approved the final manuscript.
The authors declare that they have no conflict of interest.